NMR Solution Conformation of an Antitoxic Analogue of α-Conotoxin GI: Identification of a Common Nicotinic Acetylcholine Receptor α_1-Subunit Binding Surface for Small Ligands and α-Conotoxins[†,‡]

K. Hun Mok and Kyou-Hoon Han*

Biomolecular Structure Research Unit, Korea Research Institute of Bioscience and Biotechnology, Yusong, P.O. Box 115, Taejon 305-600, Republic of Korea

Received March 10, 1999; Revised Manuscript Received July 2, 1999

ABSTRACT: The three-dimensional solution conformation of an 11-residue antitoxic analogue of α-conotoxin GI, des-Glu1-[Cys3Ala]-des-Cys13-conotoxin GI (CANPACGRHYS-NH_2, designated "GI-15" henceforth), has been determined using two-dimensional ^{1}H NMR spectroscopy. The disulfide loop region (1C−6C) and the C-terminal tail (8R−11S) are connected by a flexible hinge formed near 7G, and the pairwise backbone rmsds for the former and the latter are 0.58 and 0.65 Å, respectively. Superpositioning GI-15 with the structure of α-conotoxin GI shows that the two share an essentially identical fold in the common first disulfide loop region (1C−6C). However, the absence of the second disulfide loop in GI-15 results in segmental motion of the C-terminal half, causing the key receptor subtype selectivity residue 8R (Arg9 in α-conotoxin GI) to lose its native spatial orientation. The combined features of structural equivalence in the disulfide loop and a mobile C-terminal tail appear to be responsible for the activity of GI-15 as a competitive antagonist against native toxin. Electrostatic surface potential comparisons of the first disulfide region of GI-15 with other α-conotoxins or receptor-bound states of acetylcholine and *d*-tubocurarine show a common protruding surface that may serve as the minimal binding determinant for the neuromuscular acetylcholine receptor α_1-subunit. On the basis of the original "*Conus* toxin macrosite model" [Olivera, B. M., Rivier, J., Scott, J. K., Hillyard, D. R., and Cruz, L. J. (1991) *J. Biol. Chem. 266,* 1923−1936], we propose a revised binding model which incorporates these results.

Conotoxins are venomous peptides naturally synthesized by marine snails of the genus *Conus* (*1*−*3*), and are currently widely used as tools for studying ligand−receptor interactions in various neuromuscular and neuronal receptors and ion-gated channels (*4*). The α-conotoxins form a distinct group of such peptides, and are known to selectively inhibit the nicotinic acetylcholine receptor (nAChR),[1] the predominant excitatory neurotransmitter receptor on muscles and nerves in the peripheral nervous system (reviewed in refs *5*−*7*). Peptides which belong to the α-conotoxin family share a common two-disulfide bond framework, where the disulfide linkages are between the first and third cysteine residues, and the second and fourth cysteine residues (Table 1) (*3*, *8*). Although the α-conotoxins can be grouped into subfamilies on the basis of sequence homology and disulfide bonding patterns (Table 1), their specificities and binding affinities toward various nAChR subtypes differ widely. Differential binding may be directed toward certain nAChR subunit interfaces or toward nAChRs originating from different vertebrate organisms or even different subtypes within one organism such as neuromuscular [$(\alpha_1)_2\beta_1\gamma\delta$ or $(\alpha_1)_2\beta_1\epsilon\delta$] or neuronal [$(\alpha_3)_2(\beta_2)_3$ or $(\alpha_7)_5$] (*9*). For instance, while α-conotoxin GI and MI preferentially target the *Torpedo californica* α_1-/γ subunit interface (*10*), α-conotoxin EI preferentially binds to the α_1/δ subunit interface of the receptor (*11*). But in mammalian muscle nAChRs, the binding preference of α-conotoxins GI and MI reverses to the α_1/δ subunit interface, whereas α-conotoxin EI does not exhibit any particular binding preference in this case. Separately, α-conotoxin MII selectively blocks mammalian neuronal $(\alpha_3)_3(\beta_2)_2$ nAChR, but not its neuromuscular counterpart (*12*), as does α-conotoxin PnIA (*13*). Clearly, a detailed structural comparison of these α-conotoxins would be highly valuable as small differences in α-conotoxin sequence and structure appear to be correlated with the observed pharmacological effects.

Of all the α-conotoxins known to date, α-conotoxin GI has been studied most extensively as a prototypic example. In addition to being the first conotoxin whose NMR solution structure was determined among any conotoxin molecules (*14*, *15*), several studies including its initial biochemical

[†] This research was supported in part by Grant NB0980 from the Ministry of Science and Technology, Korea. K.H.M. is a Korea Science and Engineering Foundation (KOSEF) Postdoctoral Fellow.

[‡] The atomic coordinates for the 30 converged structures of des-Glu1-[Cys3Ala]-des-Cys13-α-conotoxin GI (GI-15) have been deposited in the Protein Data Bank, The Research Collaboratory for Structural Bioinformatics, http://www.rcsb.org/pdb/, under file name 1QS3.

* To whom correspondence should be addressed. Phone: +82 (42) 860-4251. Fax: +82 (42) 860-4259. E-mail: khhan@biotech5.kribb.re.kr.

[1] Abbreviations: ACh, acetylcholine; nAChR, nicotinic acetylcholine receptor; TC, *d*-tubocurarine; NOE, nuclear Overhauser effect; MALDI-TOF, matrix-assisted laser desorption ionization time-of-flight; CSI, chemical shift index; rMD, restrained molecular dynamics; SA, simulated annealing; T_1, spin−lattice relaxation time; T_2, spin−spin relaxation time.

10.1021/bi990558n CCC: $18.00 © 1999 American Chemical Society
Published on Web 08/24/1999

Table 1: Amino Acid Sequences of Selected Neuromuscular and Neuronal nAChR-Targeting Conotoxins

α-Conotoxin	Amino Acid Sequence [a]	References
GI	ECC NPAC GRHYS C*	*16*
MI	GRCC HPAC GKNYS C*	*28*
SI	ICC NPAC GPKYS C*	*29*
EI	RDOCCYHPTCNMSNPQIC*	*11*
MII	GCCSNPVCHLEHSNLC*	*12*
PnIA	GCCSLPPCAANNPDYC*	*13*
Analog GI-15	CA NPAC GRHYS*	*4, 30*
αA-PIVA	GCCGSYPNAACHPCSCK DROSYCGQ*	*31*
αA-EIVA	GCCGPYONAACHOCGCKVGROOYCDROSGG*	*32*

[a] The asterisk denotes an amidated C-terminus, and O denotes *trans*-4-hydroxyproline.

characterization (*16*), determination of the X-ray structure (*17*), disulfide bridge formation studies (*18*−*20*), and high-resolution NMR structure studies (*21*, *22*) have yielded information that assists in defining structure−function relationships between the α-conotoxins and the nAChR. In particular, the three-dimensional structures of conotoxin GI (*14*, *15*, *17*, *21*, *22*) and other α-conotoxins such as MII (*23*, *24*), PnIA (*25*), PnIB (*26*), and αA-conotoxin PIVA (*27*) have provided valuable structure-based insights to the understanding of receptor−ligand interactions. Site-specific mutagenesis of α-conotoxins designed to identify key determinant residues responsible for binding either the α_1/γ subunit or α_1/δ subunit interface offers an additional way of distinguishing important residues or regions for binding (*33*−*35*). For example, using site-specifically replaced residues of GI and SI, His10 and particularly Arg9 were found to be involved in the discrimination between γ- and δ-subunit affinities (*34*, *35*).

With regard to characterizing the structural determinants for binding the invariant α_1-subunit present in all neuromuscular nAChRs, a discussion (*4*) about the development of synthetic analogues of α-conotoxin GI (*30*, *36*) prompted us to consider GI-15 (termed "analog 15" in ref *4*) as a candidate worthy of high-resolution structural study (Table 1). All of the reported analogues were based on the common template of des-Glu1-conotoxin GI, as the deletion of Glu1 has a negligible effect on the toxicity of conotoxin GI (*30*, *37*). Of these analogues, GI-15 was particularly interesting due to its "antitoxic" property, the ability to antagonize lethal dosages of des-Glu1-conotoxin GI (*30*, *36*). In contrast, a single-site substitution of GI-15 (Gly8 → D-Ala; designated GI-16) reversed the antitoxic effect of GI-15, resulting in a weakly toxic peptide (*4*, *36*). In light of these pharmacological data, there appear to be important structural determinants that distinguish α-conotoxin GI from its competitive antagonist GI-15. Equally interesting would be identifying any common features between GI-15 and α-conotoxin GI, as both possess the ability to competitively bind the receptor. In the study presented here, a three-dimensional structure of GI-15 using ^{1}H two-dimensional spectroscopy combined with distance geometry, full relaxation matrix analysis, and simulated annealing is reported in an effort to address these questions. Inspection of the regions hypothesized to bind the α_1-subunit among other α-conotoxin molecules and other small molecule ligands will show a possible common structural binding surface. Finally, a revised macrosite ligand binding model for nAChR incorporating this putative common α_1-subunit binding region is presented in comparison with the original "*Conus* toxin macrosite model" (*3*, *4*).

EXPERIMENTAL PROCEDURES

Peptide Synthesis, Disulfide Bridge Formation, and Purification. GI-15 was synthesized on an Applied Biosystems/Perkin-Elmer 432A Synergy Peptide Synthesizer using FastMoc cycles (HBTU/piperidine activation, DMF/NMP/DMSO as the coupling solvent) and Synergy Fmoc-Amide resin. The peptide was cleaved by adding 1.8 mL of trifluoroacetic acid (TFA) with 0.1 mL of 1,2-ethanedithiol (EDT) and 0.1 mL of thioanisole as scavengers for 1 h, and then precipitated with 15 mL of methyl *tert*-butyl ether (MTBE) at 4 °C and centrifugation at 2000*g*. The MTBE washing was repeated three more times, and the peptide was solubilized with 20% acetic acid. The pH of the peptide solution was increased to 8.5 with NH_4OH and the mixture slowly stirred at room temperature to permit disulfide bridge formation. The progress of folding was monitored with a Vydac 214TP52 reversed-phase HPLC column (2.1 mm × 250 mm, C4, 5 μm particle and 300 Å pore sizes, respectively), using a linear gradient of 5 to 30% CH_3CN in 0.1% TFA. Alternatively, the decrease in the hydrodynamic volume of the disulfide-formed peptide was observed using a Superdex Peptide HR 10/30 (10 mm × 30 cm, Pharmacia) gel filtration column.

Purification of the peptide was performed using preparative reversed-phase HPLC. A Kromasil KR-100-10-C8 (10 mm × 250 mm, C8, 10 μm, 100 Å, Akzo Nobel) column was used, with a linear gradient of 10 to 20% CH_3CN in 0.1% TFA over 20 column volumes. The fractionated peak was checked for purity using a Vydac 218TP52 RP-HPLC column (2.1 mm × 250 mm, C8, 5 μm, 300 Å) with a linear gradient of 5 to 25% CH_3CN in 0.l % TFA. The final collection of sample was approximately 5 mg which was more than 95% pure. MALDI-TOF mass spectrometry analyses using cinnapinic acid as matrix on a Kompact Research MALDI IV instrument (Kratos Analytical) confirmed the identities of the synthesized peptide.

NMR Experiments. Samples for NMR studies were prepared in 90% H_2O/10% ^2H_2O or 100% ^2H_2O at pH 3.8 with a final sample concentration of 5 mM. NMR experiments were performed in a phase-sensitive mode (*38*) using a Varian UNITY 500 or UNITY INOVA 600 spectrometer at 4, 14, and 24 °C to obtain unambiguous resonance assignment. Solvent suppression was carried out using selective, low-power (field strength of approximately 55 Hz) irradiation of the water resonance during a relaxation delay of 1.5 s.

Solvent suppression was also applied during the mixing period for the NOESY (*39*) or ROESY (*40*, *41*) experiments. All peaks were referenced to a residual water signal (4.76 ppm at 25 °C). Mixing times of 150−500 ms for NOESY and 150−320 ms for ROESY were used. For TOCSY experiments (*42*), an 85 ms mixing time was employed. In addition, a total of eight $^3J_{HNH\alpha}$ coupling constants for the backbone torsion angle was measured from phase-sensitive DQF-COSY experiments (*43*). Also, a PE-COSY experiment (*44*) was performed in 100% ^2H_2O to measure $^3J_{\alpha\beta}$ coupling constants, which were used in conjunction with the $d_{N\beta}$ NOEs to provide χ^1 torsion angles. A typical two-dimensional data set consisted of 2048 complex points in the t_2 dimension and 256 complex t_1 increments.

Backbone dynamics of GI-15 were studied by measuring natural abundance $^{13}C_\alpha$ relaxation times using the Varian ProteinPack gradient HSQC pulse sequence (*45*). Seven different relaxation delays ranging from 5 to 485 ms for T_1 and from 5 to 230 ms for T_2 were used except for measuring relaxation times of 7G where shorter relaxation periods of 5−245 ms for T_1 and 5−95 ms for T_2 were employed. The resonance assignment of $^{13}C_\alpha$ was achieved using a two-dimensional HSQC-TOCSY experiment (*46*) and the results of ^{1}H resonance assignment. T_1 and T_2 values were determined by fitting measured peak heights to single-exponential decay curves using Kaleidagraph version 2.1.3 (Abelbeck Software). Data acquisition, sequential assignments, and spectral interpretation were performed on SPARCstation IPX or Ultra 1 Creator workstations (Sun Microsystems) running VnmrX 6.1A software (Varian Associates, Inc.).

Computation of Structures. Two-dimensional NMR data were processed using the Felix 95.0 module of Insight II 97.0 (Biosym/MSI) on Indigo^2 xL or Indy workstations (Silicon Graphics). NOE interproton distance constraints were derived primarily from the NOESY spectrum recorded at 4 °C with a mixing time of 150 ms. Prior to Fourier transformation, FIDs were reconstructed using linear prediction, apodized with a 75° sine-bell window function in both dimensions, and baseline corrected using the FLATT algorithm (*47*). NOE cross-peak volumes were measured with Felix 95.0 and converted into upper bounds of interproton distances, using a distance of 1.8 Å as a reference for nonoverlapping geminal β-proton cross-peaks. To allow for volume integration errors and possible conformational averaging, 0.5 Å additions to constraints involving only backbone protons, and 1.0 Å for cases where at least one side chain proton existed, were performed. Additional allowances for pseudoatoms and pseudoatom pairs were given, ranging from 1.5 to 2.5 Å. In addition to the interproton distance restraints, dihedral angle restraints measured from $^3J_{HNH\alpha}$ and $^3J_{\alpha\beta}$ coupling constants were included for structure calculations. A total of 108 distance constraints, including nine medium-range constraints and one long-range constraint, together with two ϕ constraints and one χ^1 torsion angle constraint were used for the computation of structures.

The preliminary structures were generated using the DGII distance geometry package (*48*) included in the NMRchitect module of Insight II 97.0. An extended molecule with one disulfide bridge and a formal charge of +3 was constructed using the potentials and partial charges provided by the consistent valence force field (CVFF) (*49*). For DGII, all parameters were default values except for the initial energy setting (800 kcal/mol) and the number of steps of simulated annealing (10 000), with the step size being 2.0 ps. Full relaxation matrix analysis using MARDIGRAS version 3.2 (*50*, *51*) was performed with DGII-generated structures as initial model structures. The three-site jump model for intra- and inter-residue distances was chosen, and the noise level was estimated to be 50% of the unnormalized absolute value of the smallest peak. The estimated rotational correlation time of 2.0 ns for α-conotoxin GI (*22*) was used as the input value.

Structures were refined through restrained molecular dynamics (rMD) calculations using Discover 2.9.7 (Biosym/MSI) and Insight II 97.0. A simulated annealing (SA) schedule based on well-established protocols (*52*) was generated. The 68 ps protocol consisted of dynamics at 1000 K (50 ps), followed by gradual temperature cooling from 1000 to 300 K (incremental temperature decrease of 100 K each over 18 ps) with staggered geometric increases of force constants for NOE, covalent, and nonbonding interactions. During the final dynamics step at 300 K and subsequent minimization steps, a modified restraint file with decreased force constants for side chain interproton distances was used to allow further conformational dynamics. Energy minimization was performed twice, first with a quartic potential and then with a Lennard-Jones nonbonded potential. The van der Waals radius was initially set to 0.825, and then increased to 1.00 during the final minimization steps. A total of 100 SA rounds were run to sample sufficient conformational space.

Assessment of Structure Quality and Display of Structures. The R_a and R_b factors (*53*) were calculated using CORMA version 5.2 (*54*) for the final ensemble of 30 structures. In addition, the stereochemistry of the computed structures was analyzed with PROCHECK version 3.5 (*55*). The three-dimensional display of structures was performed using either Insight II 97.0 (Biosym/MSI) or GRASP version 1.3.6 (*56*).

Generation of nAChR-Bound ACh and TC Structures. Three-dimensional structures of acetylcholine (ACh) and *d*-tubocurarine (TC) bound to the nAChR or its α184−200 fragment were generated using the previously reported structures and interproton distances (*57*, *58*). A two-dimensional model of TC was initially built using the Builder module of Insight 97.0 (Biosym/MSI), followed by generation of the preliminary three-dimensional structure using DGII. The initial energy setting was 3000 kcal/mol; the number of steps for simulated annealing was 10 000, and the step size was 2.0 ps. The resulting structure was visually identical to the previously reported one (*58*), including the presence of severely distorted aromatic rings. To alleviate these structural abnormalities, a restrained energy minimization calculation was performed on the DGII-generated structure. Interproton distance restraints that were not dramatically affected by the free-to-bound conformational rearrangement of TC were modified to accommodate further distance violations. The minimization protocol involved an alternate application of steepest descent and conjugate gradient methods for a total of 30 000 steps. The total energy values decreased from an initial value of 7001 kcal/mol to a final value of 829.6 kcal/mol, and all of the aromatic rings appeared to be free of distortions. The three-dimensional structure of bound ACh was generated on the basis of the intact nAChR-bound ACh data (*57*).

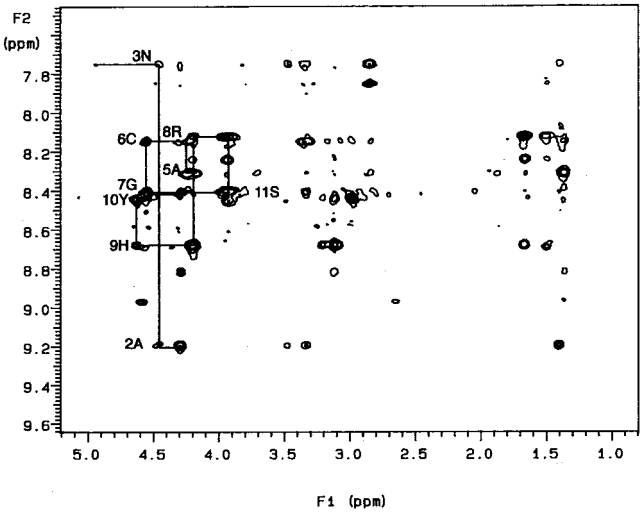

FIGURE 1: Portion of the 500 MHz two-dimensional NOESY NMR spectrum of 5 mM des-Glu1-[Cys3Ala]-des-Cys13-conotoxin GI (GI-15) obtained with a mixing time of 150 ms in 90% H_2O/10% ^2H_2O at pH 3.8 and 4 °C. The $d_{\alpha N}$ NOE cross-peaks are connected by lines, and the residues are labeled along their amide NH resonances. The presence of the 4P residue results in a broken connectivity between 3N and 5A.

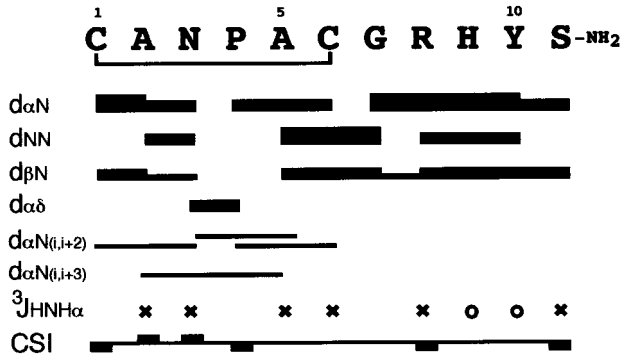

FIGURE 2: Summary of the sequential and medium-range NOE connectivities, $^3J_{HNH\alpha}$ coupling constants, and CSI values for GI-15. The thickness of the bars is proportional to the NOE intensity, classified as either strong, medium, or weak. Circles denote $^3J_{HNH\alpha}$ values of >8.0 Hz, and crosses denote residues with $^3J_{HNH\alpha}$ values of 6.0−8.0 Hz. CSI values of +1, 0, and −1 are represented as above, no indication, and below the horizontal line, respectively.

RESULTS

Resonance Assignment. The complete ^{1}H resonance assignment for GI-15 was achieved in a straightforward manner using DQF-COSY, TOCSY, and NOESY/ROESY spectra following the standard sequential assignment procedure (*59*). To prevent confusion between residue numbering of the native conotoxin sequences (Table 1) and the N-terminal des-Glu1 analogues, we will use the three-letter amino acid residue notation for the native α-conotoxin GI sequence (e.g., Cys2−Cys7 disulfide loop). On the other hand, one-letter amino acid symbols will be exclusively used for the sequence numbering of the analogues starting from the N-terminal cysteine residue (e.g., 1C−6C disulfide loop). Unambiguous assignment of some amino acids such as 8R and 9H was immediately possible by taking advantage of characteristic back-transfer cross-peaks. Once the individual spin systems were classified according to the spin systems along the NH resonances, sequential NOE cross-peaks were used to finalize the assignment. Figure 1 shows the fingerprint region of the 150 ms mixing time NOESY spectrum of GI-15 at 4 °C, and Figure 2 is a summary of sequential and medium-range NOEs used for resonance assignment along with $^3J_{HNH\alpha}$ values and the chemical shift indices (CSIs) (*60*). Except for resonance overlap between sequential $d_{\alpha N}$ NOE peaks for 7G, 10Y, and 11S with the intraresidue $d_{\alpha N}(10)$, all of the sequential NOEs were clearly resolved at 4 °C. The intraresidue $d_{\alpha N}(3)$ cross-peak and the sequential $d_{\alpha\delta}(3,4)$ cross-peak could not be observed at 4 °C due to solvent suppression, but were unambiguously detected at 14 and 24 °C to show that the 3N−4P peptide bond was in the *trans* configuration. In addition, a small number of minor cross-peaks involving 7G, 8R, and 10Y were observed.

Description of Structures. Figure 3 shows the superposition of a final ensemble of 30 structures calculated after simulated annealing refinement. Pairwise superpositioning was performed using two different regions of the peptide, one on the disulfide loop (1C−6C) and another for residues 7G−11S, as shown in panels a and b of Figure 3, respectively. It is evident that due to the absence of long-range NOE restraints between the disulfide loop and the C-terminal tail, the two regions of the molecule are structurally independent from each other, separated by a hinge near 7G. Segmental motion of the C-terminal tail relative to the disulfide loop appears to exist (see below) even though full rotational freedom around 7G is not allowed as the intraresidue $d_{\alpha N}(7)$ distance and the sequential $d_{\alpha N}(7,8)/d_{NN}(7,8)$ distances are strongly dependent upon one another. Despite torsional freedom near the hinge (Figure 3), the values obtained from angular order parameter analysis show relatively good internal agreement among the structures (Figure 4). As a result, the pairwise rmsds among the 30 final structures are quite reasonable if the disulfide loop (1C−6C) and the C-terminal tail (7G−11S) are compared separately (Figure 3) even though the overall rmsd for the entire GI-15 ensemble is relatively large (Table 2). The fact that the heavy atom rmsd for the C-terminal tail is relatively poor (2.10 Å) in contrast to the backbone rmsd value (0.645 Å) suggests that the side chain orientations of the C-terminal region are relatively disordered. The mobilities of the side chain orientations of Arg9 and His10 have been noticed in the NMR structure of α-conotoxin GI as well (*21*).

An interesting feature appears to be the occurrence of a subgroup of GI-15 structures (four out of the 30 final structures) that have their C-terminal tails in close proximity with the N-terminal residues (Figure 3a). Because GI-15 lacks the second disulfide bridge (Cys3−Cys13), the fact that the C-terminal end is able to wrap itself toward the N-terminal residues was somewhat unexpected. However, as noted in Table 2, the total energies of the individual structures within the computed ensemble are quite similar, suggesting that conformational heterogeneity is indeed possible.

Backbone Dynamics of GI-15. To gain better insight into the observed segmental motion of the C-terminal tail relative to the disulfide loop, natural abundance $^{13}C_\alpha$ T_1 and T_2 relaxation times were determined for 10 out of the 11 residues of GI-15. At 4 °C the H_α of 3N resonates close to water resonance, preventing measurement of its relaxation times. T_1 values are sensitive to motions on the scale of 10^8−10^{12} s^{-1}, while T_2 values are sensitive to dynamics on the 10^3−10^6 s^{-1} scale (*61*). As summarized in Figure 5, the T_1

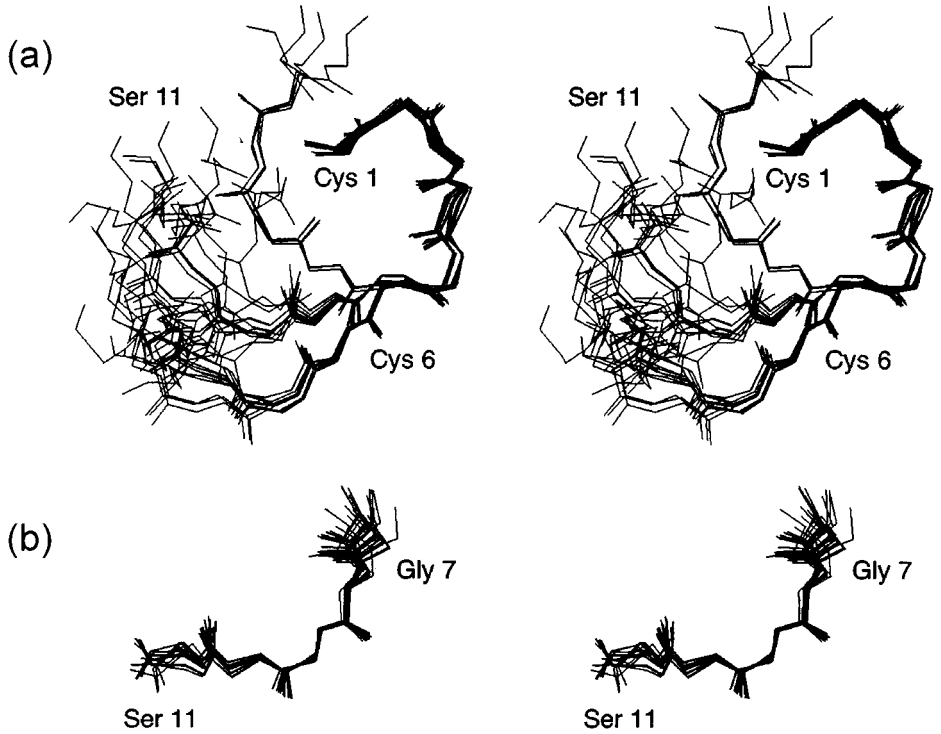

FIGURE 3: Stereoviews of the 30 final structures of GI-15 superimposed over the backbone atoms (N, C^{α}, C′, and O) of (a) residues 1−6 and (b) residues 7−11. Residues 1−6 are not shown in panel b. Selected residues are labeled.

and especially T_2 relaxation times increase progressively as one moves away from 7G. Such a trend is particularly notable for the C-terminal tail, whereas the relaxation times remain similar for all residues within the disulfide loop. The data suggest that the backbone dynamics of GI-15 point to conformational flexibility involving segmental motion of the C-terminal tail centered near 7G.

DISCUSSION

Structural Comparison with α-Conotoxin GI. Figure 6 shows ribbon diagrams of three representative structures from the GI-15 ensemble (Figure 3a) superimposed with the X-ray structure of α-conotoxin GI (*17*) (Protein Data Bank file name 1NOT) along the backbone of the Cys2−Cys7 disulfide loop. The backbone and heavy atom rmsds of superpositioned residues comprising the Cys2−Cys7 disulfide loop are 0.880 and 1.270 Å, respectively, indicating a high degree of structural equivalence between GI-15 and α-conotoxin GI in this region. Superpositioning the representative structures of GI-15 with the recently determined NMR solution structure (*21*) (Protein Data Bank file name 1XGA) results in similar agreement (data not shown). Therefore, the absence of the second disulfide bond (Cys3−Cys13), which conformationally restricts the C-terminal end of α-conotoxin GI and additionally provides long-range interactions such as Cys2−Ser12 and Glu1−Cys13 hydrogen bonding (*17*), does not appear to influence the local conformation of the Cys2−Cys7 loop.

In contrast, when the 7G−11S backbone is superimposed with the corresponding Gly8−Ser12 segment in the X-ray structure of α-conotoxin GI, the rmsd amounts to a relatively high value of 1.627 Å. The same superpositioning of this region between GI-15 and the NMR structure of α-conotoxin GI (*21*) is similarly high (1.659 Å), confirming the role of the Cys3−Cys13 disulfide bridge on the backbone fold (*17*, *21*), toxin activity (*19*), and subunit selectivity of α-conotoxin GI (*21*). As noted above, a small subgroup population (∼10% within the ensemble) of GI-15 structures have their C-terminal tails in close proximity with the N-terminal residues (Figure 3a), suggesting that a native α-conotoxin GI-like fold may be possible for GI-15. In fact, the side chain of the receptor-binding residue Arg9 points in the opposite direction with respect to that of α-conotoxin GI (Figure 6). This is also the case when comparing GI-15 with the α-conotoxin GI NMR solution structure ensemble (*21*), where Arg9 is particularly shown to be mobile. GI-15 therefore seems to have lost the "selectivity face" (*21*), a region of residues known to target the non-α_1 subunit interface of the nAChR.

In vitro activity and in vivo antagonistic activity assays on the six-residue disulfide-looped analogue Cys2-Ala3-Asn4-Pro5-Ala6-Cys7-NH_2 ("analog 11" from ref *36*) demonstrated neither toxic nor antitoxic activity, indicating that the N-terminal disulfide loop alone cannot inhibit the toxin's action (*36*). It is when successive α-conotoxin GI residues are attached to the N-terminal (Gly8, then Arg9, then His10, etc.) that the fraction of antitoxic activity increases, finally reaching its maximum with the structure of GI-15 (*36*). Thus, segmental mobility notwithstanding, the C-terminal tail appears to contribute to the antitoxic activity of GI-15 in some yet-undetermined way. In light of the facts that α-conotoxins are rigid three-dimensional scaffolds stabilized by disulfide bridges, and that each has a small but distinct number of variable residues that confer species and receptor subtype selectivity (*4*), preserving the first disulfide loop while allowing flexibility for toxicity-conferring residues may be a viable solution for obtaining antitoxic properties otherwise difficult within a given ligand-binding pocket.

Identification of a Common Binding Surface among Various Ligands. The CC(N/H)PAC motif is commonly found in all members of the α-conotoxin α3/5 subfamily

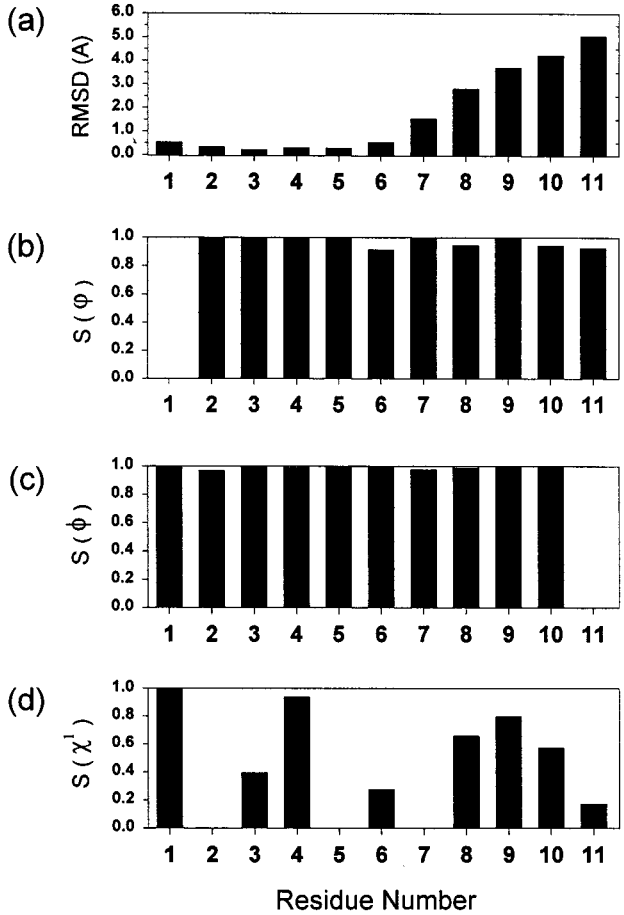

FIGURE 4: Plots as a function of residue number of (a) the average rmsd for the backbone heavy atoms when superimposed over residues 1−6 and (b−d) the angular order parameters for the backbone and first side chain dihedral angles.

Table 2: NMR Structure Determination Statistics of GI-15 for an Ensemble of 30 Structures[a]

rms deviations from experimental restraints	
interproton distances (Å)	0.0586 ± 0.003
maximum NOE violation (Å)	1.039
maximum torsional angle violation (deg)	0.12
energies	
mean total energy (kcal/mol)	172.14 ± 2.51
mean constraint violation energy (kcal/mol)	6.65 ± 2.95
Ramachandran plot statistics	
no. of residues in the most favored region (%)	54.9
no. of residues in additionally allowed region (%)	44.0
no. of residues in generously allowed region (%)	1.1
no. of residues in disallowed region (%)	0.0
ensemble *R* factors[b]	
R_a	0.527 ± 0.026
R_b	0.138 ± 0.005
rms deviations from the average structure	
disulfide loop (1−6)	
backbone atoms[c]/heavy atoms (Å)	0.580/0.987
C-terminal tail (7−11)	
backbone atoms/heavy atoms (Å)	0.645/2.100
entire chain (1−11)	
backbone atoms/heavy atoms (Å)	1.929/2.869

[a] Values where applicable are means ± standard deviations. [b] R_a and R_b values are computed as defined by Thomas et al. (*53*). [c] Backbone atoms are C^α, N, C′, and O.

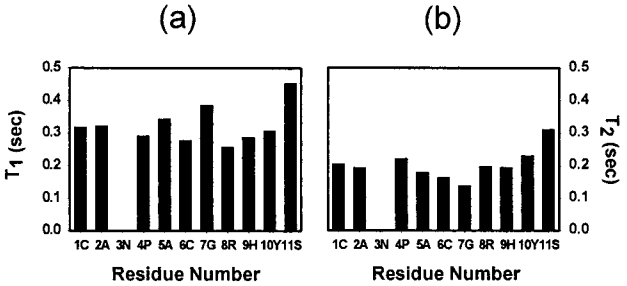

FIGURE 5: Plots of backbone (a) T_1 and (b) T_2 $^{13}C_\alpha$ relaxation times against the sequence of GI-15. The $^{13}C_\alpha$ relaxation times for 3N could not be measured because the H_α resonates too close to the water resonance.

(Table 1) (*4*). On the basis of the cumulative data, the CC(N/H)PAC motif of the α3/5 subfamily has been hypothesized to bind the α_1-subunit of the nAChR (*21*). A recent high-resolution NMR structural study of α-conotoxin EI (K. Han, unpublished results), which preferentially targets the neuromuscular nAChR α_1/δ subunit interface but belongs to the α 4/7 subfamily instead of the α3/5 subfamily, suggests the homologously positioned His7-Pro8-Thr9 segment (Table 1) to be the putative α_1-subunit binding region even in the α4/7 subfamily. Another α-conotoxin subfamily known as the αA-conotoxins, though possessing a completely different disulfide bridge framework (Table 1), attacks both α_1/γ and α_1/δ subunit interfaces of the neuromuscular nAChR (*32*). The common structural features among the α- and αA-conotoxins responsible for binding to the invariant nAChR α_1-subunit has yet to be established.

Equally important when probing the neuromuscular nAChR binding site should be structural comparisons of the conformations of ligands other than the α- or αA-conotoxins such as ACh and TC, a strong antagonist of the nAChR frequently used in probing ligand−nAChR interactions. The solution conformations of ACh bound to the whole *T. californica* nAChR (*57*) or alternatively to the α_1-subunit fragment consisting of residues 184−200 (*58*) have been studied using two-dimensional NMR. In both cases, ACh adopts a conformation where the quaternary ammonium methyl groups form a hydrophobic surface separated from negatively charged acetyl oxygen atoms (*57*). The solution conformation of TC bound to the α_1-subunit 184−200 fragment of nAChR has also been studied using transferred NOE (*58*). Extensive conformational change is observed upon binding to the receptor fragment, resulting in a positively charged hydrophobic segment formed by the quaternary ammonium methyl groups, with dimensions similar to those of the bound ACh structure.

In Figure 7, we show electrostatic potential surfaces generated by GRASP (*56*) for ACh and TC (both receptor-bound states), the α-conotoxins GI, GI-15, and EI and αA-conotoxin PIVA to elucidate potentially similar structural regions. The electrostatic potential surface of the heat-stable enterotoxin (ST) Mpr^5-ST_p(5−17) (*62*) is also shown, as the CC(N/H)PAC sequence is present in this peptide as well (*21*). For the cases of the α-conotoxins and enterotoxin, a common weakly positively charged hydrophobic surface consisting of two protruding lobes interacting at right angles is generated by adjacent or nearby Pro and Ala/Thr residues. The horizontal lobe, formed by the Ala/Thr residue, is positioned slightly underneath the vertical lobe, which is the Pro side chain. The indicated Pro and Ala/Thr residues are all present within the putative CC(N/H)P(A/T)C α_1-subunit binding consensus sequence (Table 1), with the exception

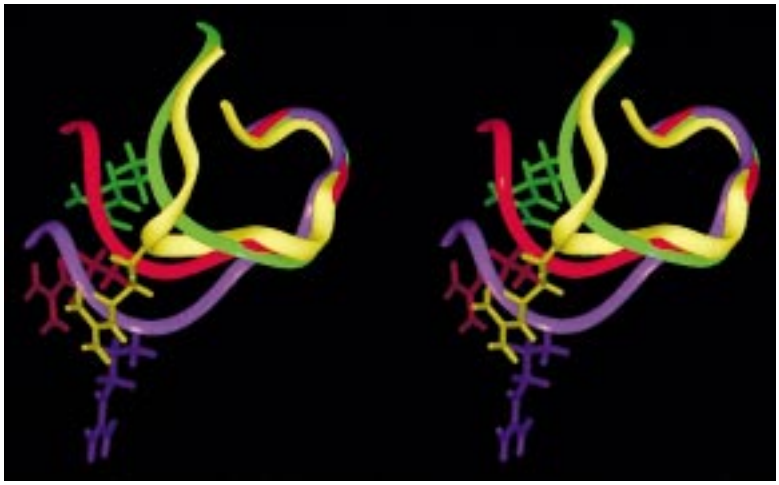

FIGURE 6: Stereoview ribbon diagrams of the backbone of three representative GI-15 structures (green, red, and purple) and the X-ray structure of α-conotoxin GI (yellow, PDB file name 1NOT; *17*). Superimposition was achieved along the Cys2−Cys7 disulfide loop of α-conotoxin GI against the (1C−6C) loop in GI-15. The side chains of the Arg9 residue are shown.

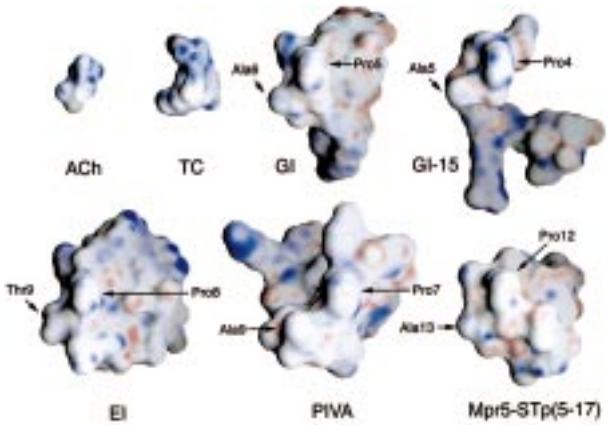

FIGURE 7: Electrostatic surface potential representations of ACh, TC, α-conotoxins GI and GI-15, EI, αA-conotoxin PIVA, and enterotoxin Mpr^5-ST_p(5−17). The structures are oriented so that the putative common α_1-subunit binding surface, which is comprised of two lobes joined at right angles and the pocket surface formed by them, can be directly viewed. The protruding common surfaces are aligned horizontally to aid in visual identification. Regions of the surface with electrostatic potentials greater than $+15kT$, equal to 0, and less than $-15kT$ are colored blue, white, and red, respectively. The atomic charges were taken from the CVF (*49*), and the calculations and generation of the diagram were performed with GRASP (*56*). α- and αA-conotoxin and enterotoxin residues that constitute the putative binding surface are labeled.

of αA-conotoxin PIVA. Interestingly, the Pro5 and Ala6 residues are adjacent in sequence in α-conotoxin GI, GI-15, and Mpr^5-ST_p(5−17), whereas α-conotoxin EI has a Ala → Thr substitution. Furthermore, in αA-conotoxin PIVA, Pro7 and Ala9 are separated by an additional residue. Hence, our analyses of the electrostatic potential surfaces show that the putative common α_1-subunit binding motif need not originate exactly from the CC(N/H)P(A/T)C sequence as long as the Pro side chain is interacting with a C_β-possessing amino acid residue within the given orientation. Biochemically, the importance of the Pro side chain is further evidenced by the complete loss of activity for the des-Glu1-[Pro5Gly]-α-conotoxin GI (*30*, *36*) and the [Pro6Gly]-α-conotoxin MI analogues (*33*). Despite the two intact native disulfide bridges, these analogues nevertheless fail to exhibit any toxic or antitoxic effects.

The putative α_1-subunit binding surface can also be found in the small molecule ligands ACh and TC, despite their marked size difference from the α- or αA-conotoxins. Due to the smaller total surface area of ACh and TC, the calculated electrostatic potential surrounding the two lobes appears to be slightly more positive than those in the peptide toxins. Nevertheless, the spatial orientation of the two lobes in ACh and TC is the same as in the α-conotoxins. Such specific orientation of the two lobes could be observed only in the three-dimensional structures of the bound states of ACh and TC (*57*, *58*). The underlying vertexes that constitute the protruding surface of ACh are one methyl group bound to the quaternary nitrogen atom, one methylene group, and the acetyl methyl group. In the case of TC, the "induced cup shape" (*58*) of the molecule allows for a phenolic ring carbon to serve as one vertex of the surface, while the quaternary nitrogen methyl group and a methoxy group comprise the other vertexes. In contrast, the same surface for the peptidic ligands and enterotoxin results from the C_β methyl/methylene group of Ala/Thr and the C_β and C_γ ring methylene groups of Pro. Not only do the surfaces appear to be similar to one another, but the distance between the Ala/Thr C_β and Pro C_γ atoms is also consistently 5.7−6.2 Å regardless of the identity of the ligand. The distance between comparable vertexes of TC falls within this range at 6.0 Å. The distance between the acetyl methyl group and quaternary nitrogen methyl group of ACh is slightly shorter, being 5.4 Å. However, a distance of 5.7 Å appears to be easily achievable without large changes in conformational energy due to the torsional freedom that is available for ACh (*57*).

Calculation of electrostatic surface potentials with GRASP (*56*) shows that quaternary ammonium groups and their attached methyl groups present in ACh and TC can take on weakly positively charged hydrophobic surfaces similar to that of the Ala/Thr and Pro side chains present in the CC(N/H)P(A/T)C-like sequence of α- or αA-conotoxin. Hence, in terms of shape, size, surface properties, and sequence for the case of peptides, the common protruding surface found for ACh, TC, or α- or αA-conotoxin appears to be very likely to interact with a common region found on the α_1-subunit of the nAChR. Consistent with this finding is the previous observation that interactions of TC, ACh, and α-conotoxin

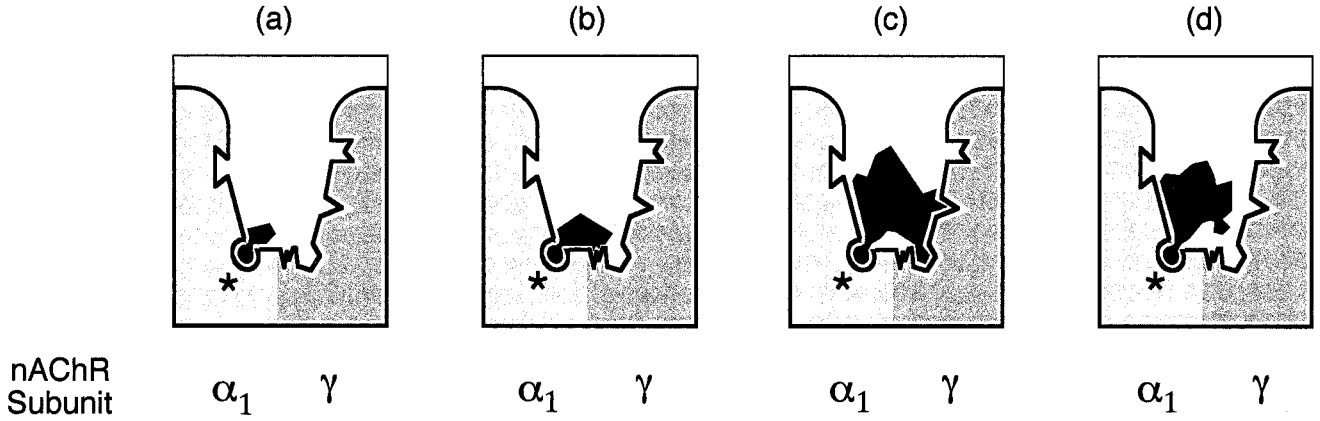

FIGURE 8: Revised schematic diagram of the original macrosite hypothesis (*3*) for ligands binding to the neuromuscular nAChR. The ligands are shown in black and are as follows: (a) ACh, (b) TC, (c) α-conotoxin GI, and (d) GI-15. The agonist binding site is denoted with the asterisk. The invariant α_1-subunit binding site is shared among all ligands, while the interaction with either the γ-subunit or the δ-subunit (not shown) depends on other binding determinants. The common α_1-subunit binding surface is schematically shown as the round projection existing in all ligands. The Arg9 residue of α-conotoxin GI is shown as a four-sided projection interacting with the *T. californica* species γ-subunit, which, in GI-15 (d), is highly mobile and does not appear to make contact with the Arg9-binding site in the γ subunit of nAChR. The binding site for TC on the γ-subunit is shown separately, as experimental data suggest that the receptor residues responsible for binding TC may be different from those of the α-conotoxins (*65*, *66*).

MI with receptor α_1-subunit residues are mediated by common residues such as Tyr190, Tyr198, and Tyr93 (*63*, *64*). The importance of satisfying all four factors, shape, size, surface property, and sequence, is evident when considering the case of the enterotoxin Mpr^5-$ST_p(5-17)$, implicated in enterotoxicity (*62*). The distributions of positive and negative electrostatic surface potentials of Mpr^5-$ST_p(5-17)$ are clearly different from those of the α- and αA-conotoxins, ACh, and TC. In addition, whereas an "armpit-like pocket" is clearly formed by the perpendicular lobes of ACh, TC, and the α- and αA-conotoxins, no appreciable pocket-like space is found in the same region for Mpr^5-$ST_p(5-17)$. These structural features seem to explain why Mpr^5-$ST_p(5-17)$, having surface contour and sequence similar to those of the α-conotoxins, is not an antagonist for the neuromuscular nAChR.

Revision of the "Macrosite Binding Hypothesis". Numerous studies on the binding specificities between the α_1/γ and α_1/δ subunit interfaces of the neuromuscular nAChR have shown a great deal of complexity among various α-conotoxins. Interestingly, nonequivalent binding between the subunit interfaces has also been observed for the small antagonist molecules. For example, unlike α-conotoxins GI and MI, TC and dimethyl-*d*-tubocurarine prefer binding the α_1/γ site to the α_1/δ site in both *T. californica* and mouse muscle receptors (*65*, *66*). This consistent subunit binding preference of γ over δ of TC toward neuromuscular nAChRs regardless of its origin indicates that TC behaves differently from α-conotoxins GI or MI in terms of the subunit selectivity. Despite the above-mentioned differences, however, a common factor among these ligands is that they all must interact with the α_1-subunit interface of nAChR. Thus, a comparison of the structural details of the ligands along with pharmacological data obtained with various site-directed mutants should in principle provide us with the common structural features present in all ligands. The availability of the solution structure of GI-15, which acts as a competitive antagonist against α-conotoxin GI, becomes valuable in this aspect since in GI-15 only the "selectivity face" (*21*, *34*, *35*) is effectively rendered inactive with minimal change in the amino acid sequence without creating any unforeseen substitution-induced effects.

An intuitive structural model describing interactions between nAChR and α-conotoxins, including the antitoxic GI-15, called the "macrosite binding hypothesis model", was previously proposed when high-resolution structures of α- or αA-conotoxins that are now known were not available (*3*, *4*). This original model suggests that when a toxin is bound to nAChR the agonist-binding site would be blocked such that ACh is unable to reach its binding site. Antitoxin, by virtue of its different conformation, was hypothesized to not only physically block the toxin from binding in a competitive fashion but also simultaneously permit unimpeded binding of the endogenous ligand ACh (*4*). Now, with the NMR structural information for the antitoxin GI-15 and the three-dimensional models of other α- and αA-conotoxins and small molecule ligands, we are able to refine the original model. Figure 8 is a schematic view of the common modes of binding of the four ligands ACh, TC, α-conotoxin GI, and GI-15 with the α_1-subunit binding surface. The identification of a common binding surface suggests that a region on the α_1-subunit is shared among these ligands. As ACh is relatively smaller than the other ligands, the proposed common binding surface in ACh must be the minimum common denominator in terms of binding the α_1-subunit. Binding of nAChR-targeting ligands other than ACh should involve both α_1-subunit and non-α_1-subunit.

Further evidence supporting the revised model is as follows. While most of the previously characterized α-conotoxins and curare-type molecules exhibit preferential binding for one subunit interface over another (*11*, *34*, *35*) such a preference is not observed for ACh or other agonists such as carbamylcholine, which are known to bind the two different subunit interfaces with equal affinities (*7*). In other words, any contribution of the non-α_1-subunit to the binding of endogenous agonist appears to be minimal. Also, the cholinergic binding site, which has been deduced from extensive receptor mutational studies, encompasses residues 184−200 of the α_1-subunit of the nAChR (*67*). Hence, the common minimal binding region between ACh, TC, α-cono-

toxin GI, and GI-15 is most likely to reside only in the α_1-subunit of the nAChR. As a result, in contrast to an unimpeded approach of ACh to the receptor's ligand binding site in the presence of GI-15 as hypothesized in the original model (*4*), competitive binding kinetics appears to be the key factor in determining which ligand, be it agonist, antagonist, or antitoxin, is able to bind to the receptor. GI-15 appears to exhibit intermediate affinities toward the receptor, acting as an antagonist toward strongly binding conotoxin peptides, yet kinetically allowing endogenous ACh to bind under appropriate conditions.

In summary, using the NMR structure of an antitoxic analogue of α-conotoxin GI, we have been able to identify a putative nAChR α_1-subunit binding surface that appears to exist in all neuromuscular nAChR-targeting conotoxins and small ligands. Further investigation will be required to determine if this common binding surface is also found in other ligands, or alternatively if this region structurally varies depending on the subtype of the target nAChR (e.g., α_1−α_9).

ACKNOWLEDGMENT

We thank Mr. Dong-Ho Choung, Mr. Kyu Hwan Park, and Ms. Jae Eun Suk for technical assistance in carrying out either the NMR experiments or the structure computations. We also thank Professor Thomas L. James for the CORMA and MARDIGRAS software packages and Professor Barry Honig and Dr. Anthony Nicholls for kindly providing the GRASP software. The GI-15 peptide was synthesized and purified at the R&D Center of the Cheil Jedang Corp. (Ichon, Korea).

SUPPORTING INFORMATION AVAILABLE

^{1}H resonance assignments for des-Glu1-[Cys3Ala]-des-Cys13-α-conotoxin GI (GI-15) at 4 °C and pH 3.8. This material is available free of charge via the Internet at http://pubs.acs.org.

REFERENCES

1. Olivera, B. M., Gray, W. R., Zeikus, R., McIntosh, J. M., Varga, J., Rivier, J., de Santos, V., and Cruz, L. J. (1985) *Science 230*, 1338−43.
2. Olivera, B. M., Rivier, J., Clark, C., Ramilo, C. A., Corpuz, G. P., Abogadie, F. C., Mena, E. E., Woodward, S. R., Hillyard, D. R., and Cruz, L. J. (1990) *Science 249*, 257−63.
3. Olivera, B. M., Rivier, J., Scott, J. K., Hillyard, D. R., and Cruz, L. J. (1991) *J. Biol. Chem. 266*, 22067−70.
4. Myers, R. A., Cruz, L. J., Rivier, J. E., and Olivera, B. M. (1993) *Chem. Rev. 93*, 1923−36.
5. Karlin, A., and Akabas, M. H. (1995) *Neuron 15*, 1231−44.
6. Aidley, D. J., and Stanfield, P. R. (1996) *Ion Channels: Molecules in Action*, Cambridge University Press, Cambridge, U.K.
7. Hucho, F., Tsetlin, V. L., and Machold, J. (1996) *Eur. J. Biochem. 239*, 539−57.
8. Myers, R. A., Zafarella, G. C., Gray, W. R., Abbott, J., Cruz, L. J., and Olivera, B. M. (1991) *Biochemistry 30*, 9370−7.
9. Sargent, P. B. (1993) *Annu. Rev. Neurosci. 16*, 403−43.
10. Hann, R. M., Pagán, O. R., and Eterović, V. A. (1994) *Biochemistry 33*, 14058−63.
11. Martinez, J. S., Olivera, B. M., Gray, W. R., Craig, A. G., Groebe, D. R., Abramson, S. N., and McIntosh, J. M. (1995) *Biochemistry 34*, 14519−26.
12. Cartier, G. E., Yoshikami, D., Gray, W. R., Luo, S., Olivera, B. M., and McIntosh, J. M. (1996) *J. Biol. Chem. 271*, 7522−8.
13. Fainzilber, M., Hasson, A., Oren, R., Burlingame, A. L., Gordon, D., Spira, M. E., and Zlotkin, E. (1994) *Biochemistry 33*, 9523−9.
14. Kobayashi, Y., Ohkubo, T., Kyogoku, Y., Nishiuchi, Y., Sakakibara, S., Braun, W., and Gō, N. (1989) *Biochemistry 28*, 4853−60.
15. Pardi, A., Galdes, A., Florance, J., and Maniconte, D. (1989) *Biochemistry 28*, 5494−501.
16. Gray, W. R., Luque, A., Olivera, B. M., Barrett, J., and Cruz, L. J. (1981) *J. Biol. Chem. 256*, 4734−40.
17. Guddat, L. W., Martin, J. A., Shan, L., Edmunson, A. B., and Gray, W. R. (1996) *Biochemistry 35*, 11329−35.
18. Gray, W. R., Luque, F. A., Galyean, R., Atherton, E., Sheppard, R. C., Stone, B. L., Reyes, A., Alford, J., McIntosh, M., Olivera, B. M., Cruz, L. J., and Rivier, J. (1984) *Biochemistry 23*, 2796−802.
19. Nishiuchi, Y., and Sakakibara, S. (1982) *FEBS Lett. 148*, 260−2.
20. Zhang, R., and Snyder, G. H. (1991) *Biochemistry 30*, 11343−8.
21. Gehrmann, J., Alewood, P. F., and Craik, D. J. (1998) *J. Mol. Biol. 278*, 401−15.
22. Maslennikov, I. V., Sobol, A. G., Gladky, K. V., Lugovskoy, A. A., Ostrovsky, A. G., Tsetlin, V. I., Ivanov, V. T., and Arseniev, A. S. (1998) *Eur. J. Biochem. 254*, 238−47.
23. Shon, K.-J., Koerber, S. C., Rivier, J. E., Olivera, B. M., and McIntosh, J. M. (1997) *Biochemistry 36*, 15693−700.
24. Hill, J. M., Oomen, C. J., Miranda, L. P., Bingham, J.-P., Alewood, P. F., and Craik, D. J. (1998) *Biochemistry 37*, 15621−30.
25. Hu, S.-H., Gehrmann, J., Guddat, L. W., Alewood, P. F., Craik, D. J., and Martin, J. L. (1996) *Structure 4*, 417−23.
26. Hu, S.-H., Gehrmann, J., Alewood, P. F., Craik, D. J., and Martin, J. L. (1997) *Biochemistry 36*, 11323−30.
27. Han, K., Hwang, K.-J., Kim, S.-M., Kim, S.-K., Gray, W. R., Olivera, B. M., Rivier, J. E., and Shon, K.-J. (1997) *Biochemistry 36*, 1669−77.
28. McIntosh, M., Cruz, L. J., Hunkapiller, M. W., Gray, W. R., and Olivera, B. M. (1982) *Arch. Biochem. Biophys. 218*, 329−34.
29. Zafaralla, G. C., Ramilo, C., Gray, W. R., Karlstrom, R., Olivera, B. M., and Cruz, L. J. (1988) *Biochemistry 27*, 7102−5.
30. Almquist, R. G., Kadambi, S. R., Yasuda, D. M., Weitl, F. L., Polgar, W. E., and Toll, L. R. (1989) *Int. J. Pept. Protein Res. 34*, 455−62.
31. Hopkins, C., Grilley, M., Miller, C., Shon, K.-J., Cruz, L. J., Gray, W. R., Dykert, J., Rivier, J., Yoshikami, D., and Olivera, B. M. (1995) *J. Biol. Chem. 270*, 22361−7.
32. Jacobsen, R., Yoshikami, D., Ellison, M., Martinez, J., Gray, W. R., Cartier, G. E., Shon, K.-J., Groebe, D. R., Abramson, S. N., Olivera, B. M., and McIntosh, J. M. (1997) *J. Biol. Chem. 272*, 22531−7.
33. Hashimoto, K., Uchida, S., Yoshida, H., Nishiuchi, Y., Sakakibara, S., and Yukari, K. (1985) *Eur. J. Pharmacol. 118*, 351−4.
34. Groebe, D. R., Gray, W. R., and Abramson, S. N. (1997) *Biochemistry 36*, 6469−74.
35. Hann, R. M., Pagán, O. R., Gregory, L. M., Jácome, T., and Eterović, V. A. (1997) *Biochemistry 36*, 9051−6.
36. Almquist, R. G., Kadambi, S. R., Yasuda, D. M., Weitl, F. L., Polgar, W., Toll, L. R., and Uyeno, E. T. (1990) in *Peptides: Chemistry, Structure and Biology* (Rivier, J., and Marshall, G. R., Eds.) pp 505−7, ESCOM, Leiden, The Netherlands.
37. Gray, W. R., Olivera, B. M., and Cruz, L. J. (1988) *Annu. Rev. Biochem. 57*, 665−700.
38. States, D. J., Haberkorn, R. A., and Ruben, D. J. (1982) *J. Magn. Reson. 48*, 286−92.
39. Jeener, J., Meier, B. H., Bachmann, P., and Ernst, R. R. (1979) *J. Chem. Phys. 71*, 4546−53.

40. Bothner-By, A. A., Stephens, R. L., Lee, J., Warren, C. D., and Jeanloz, R. W. (1984) *J. Am. Chem. Soc. 106*, 811.
41. Griesinger, C., and Ernst, R. R. (1987) *J. Magn. Reson. 75*, 261−71.
42. Griesinger, C., Otting, G., Wüthrich, K., and Ernst, R. R. (1988) *J. Am. Chem. Soc. 110*, 7870−2.
43. Rance, M., Sorenson, D. W., Bodenhausen, G., Wagner, G., Ernst, R. R., and Wüthrich, K. (1983) *Biochem. Biophys. Res. Commun. 117*, 479−85.
44. Mueller, L. (1987) *J. Magn. Reson. 72*, 191−6.
45. Kay, L. E., Keifer, P., and Saarinen, T. (1992) *J. Am. Chem. Soc. 114*, 10663−5.
46. John, B. K., Plant, D., Heald, S. L., and Hurd, R. E. (1991) *J. Magn. Reson. 94*, 664−9.
47. Güntert, P., and Wüthrich, K. (1992) *J. Magn. Reson. 96*, 403−7.
48. Havel, T. F. (1991) *Prog. Biophys. Mol. Biol. 56*, 43−78.
49. Dauber-Osguthorpe, P., Roberts, V. A., Osguthorpe, D. J., Wolff, J., Genest, M., and Hagler, A. T. (1988) *Proteins: Struct., Funct., Genet. 4*, 31−47.
50. Borgias, B. A., and James, T. L. (1989) *Methods Enzymol. 176*, 169−83.
51. Borgias, B. A., and James, T. L. (1990) *J. Magn. Reson. 87*, 475−87.
52. Nilges, M., Clore, G. M., and Gronenborn, A. M. (1988) *FEBS Lett. 239*, 129−36.
53. Thomas, P. D., Basus, V. J., and James, T. L. (1991) *Proc. Natl. Acad. Sci. U.S.A. 88*, 1237−41.
54. Keepers, J. W., and James, T. L. (1984) *J. Magn. Reson. 57*, 404−26.
55. Laskowski, R. A., MacArthur, M. W., Moss, D. S., and Thornton, J. M. (1993) *J. Appl. Crystallogr. 26*, 283−91.
56. Nicholls, A., Sharp, K. A., and Honig, B. (1991) *Proteins: Struct., Funct., Genet. 11*, 281−96.
57. Behling, R. W., Yamane, T., Navon, G., and Jelinski, L. W. (1988) *Proc. Natl. Acad. Sci. U.S.A. 85*, 6721−5.
58. Fraenkel, Y., Gershoni, J. M., and Navon, G. (1994) *Biochemistry 33*, 644−50.
59. Billeter, M., Braun, W., and Wüthrich, K. (1982) *J. Mol. Biol. 155*, 321−46.
60. Wishart, D. S., and Sykes, B. D. (1994) *Methods Enzymol. 239*, 363−92.
61. Kay, L. E., Torchia, D. A., and Bax, A. (1989) *Biochemistry 28*, 8972−9.
62. Ozaki, H., Sato, T., Kubota, H., Hata, Y., Katsube, Y., and Shimonishi, Y. (1991) *J. Biol. Chem. 266*, 5934−41.
63. Sine, S. M., Quiram, P., Papanikolaou, F., Kreienkamp, H.-J., and Taylor, P. (1994) *J. Biol. Chem. 269*, 8808−16.
64. Sugiyama, N., Marchot, P., Kawanishi, C., Osaka, H., Molles, B., Sine, S. M., and Taylor, P. (1998) *Mol. Pharmacol. 53*, 787−94.
65. Pedersen, S. E., and Cohen, J. B. (1990) *Proc. Natl. Acad. Sci. U.S.A. 87*, 2785−9.
66. Fu, D.-X., and Sine, S. M. (1994) *J. Biol. Chem. 269*, 26152−7.
67. Neumann, D., Barchan, D., Fridkin, M., and Fuchs, S. (1986) *Proc. Natl. Acad. Sci. U.S.A. 83*, 9250−3.

BI990558N